Acta Pharmaceutica Sinica B 2022;12(1):353−363

Chinese Pharmaceutical Association
Institute of Materia Medica, Chinese Academy of Medical Sciences

Acta Pharmaceutica Sinica B

www.elsevier.com/locate/apsb
www.sciencedirect.com

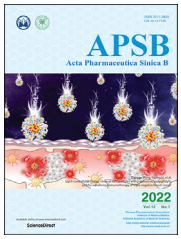

ORIGINAL ARTICLE

Light-controllable charge-reversal nanoparticles with polyinosinic-polycytidylic acid for enhancing immunotherapy of triple negative breast cancer

Lei Fang[a,b], Zitong Zhao[b], Jue Wang[b], Ping Xiao[b], Xiangshi Sun[b], Yaping Ding[a], Pengcheng Zhang[b,d], Dangge Wang[b,c,d,*], Yaping Li[b,c,d,*]

[a]*Collage of Sciences, Shanghai University, Shanghai 200444, China*
[b]*State Key Laboratory of Drug Research & Center of Pharmaceutics, Shanghai Institute of Materia Medica, Chinese Academy of Sciences, Shanghai 201203, China*
[c]*School of Pharmacy, Yantai University, Yantai 264005, China*
[d]*Yantai Key Laboratory of Nanomedicine & Advanced Preparations, Yantai Institute of Materia Medica, Yantai 264000, China*

Received 14 March 2021; received in revised form 18 April 2021; accepted 26 April 2021

KEY WORDS

Nanoparticles;
Cancer immunotherapy;
Photodynamic therapy;
Polyinosinic-polycytidylic acid;
Triple negative breast cancer;
Charge-reversal;
Tumor microenvironment;
ROS-responsive

Abstract Nucleic acid drugs are highly applicable for cancer immunotherapy with promising therapeutic effects, while targeting delivery of these drugs to disease lesions remains challenging. Cationic polymeric nanoparticles have paved the way for efficient delivery of nucleic acid drugs, and achieved stimuli-responsive disassembly in tumor microenvironment (TME). However, TME is highly heterogeneous between individuals, and most nanocarriers lack active-control over the release of loaded nucleic acid drugs, which will definitely reduce the therapeutic efficacy. Herein, we have developed a light-controllable charge-reversal nanoparticle (LCCN) with controlled release of polyinosinic-polycytidylic acid [Poly(I:C)] to treat triple negative breast cancer (TNBC) by enhanced photodynamic immunotherapy. The nanoparticles keep suitably positive charge for stable loading of Poly(I:C), while rapidly reverse to negative charge after near-infrared light irradiation to release Poly(I:C). LCCN-Poly(I:C) nanoparticles trigger effective phototoxicity and immunogenic cell death on 4T1 tumor cells, elevate anti-tumor immune responses and inhibit the growth of primary and abscopal 4T1 tumors in mice. The

*Corresponding authors. Tel./fax: +86 21 20231979 (Yaping Li); +86 21 20231979 (Dangge Wang).
E-mail addresses: dgwang@simm.ac.cn (Dangge Wang), ypli@simm.ac.cn (Yaping Li).

Peer review under responsibility of Chinese Pharmaceutical Association and Institute of Materia Medica, Chinese Academy of Medical Sciences.

https://doi.org/10.1016/j.apsb.2021.06.006

approach provides a promising strategy for controlled release of various nucleic acid-based immune modulators, which may enhance the efficacy of photodynamic immunotherapy against TNBC

1. Introduction

Triple negative breast cancer (TNBC) is one of the most aggressive subtypes of breast cancer with highly invasive and metastatic properties[1,2]. Chemotherapy is the major clinically available approach for treating TNBC[1,3]. However, it fails to benefit a large proportion of patients with TNBC due to nonspecific drug distribution off tumors and severe adverse effects[4,5]. In past decades, cancer immunotherapy has made great progress in treating advanced TNBC tumors[6–8]. Prolonged progression-free survival in patients with advanced breast cancer has been achieved by using pembrolizumab plus chemotherapy[9]. Despite promising, low immunogenicity and immunosuppressive tumor microenvironment (TME) remain major obstacles for most immunotherapies when treating TNBC[10,11]. Therefore, effective approaches that improve tumor immunogenicity as well as reverse immunosuppressive factors are highly desirable for enhanced immunotherapy of TNBC.

A diversity of nanoparticles has been reported to trigger the immunogenicity of tumors with improved therapeutic efficacy[12]. The nanoparticles are designed with intelligent moieties to change their shape, size and surface characteristics according to inner or external stimuli for precisely controlled drug delivery. Among them, charge-reversal nanoparticles are widely used to avoid clearance by the reticuloendothelial system, enhance tumor-specific accumulation, penetration and cellular uptake[13–15]. For example, an acidity-responsive cisplatin-loaded nanocarrier was fabricated to treat cisplatin-resistant tumor with ultrafast charge conversion property[13]. A polymeric prodrug micelle with charge-reversal and self-amplifiable drug release properties was constructed to overcome multidrug resistance. The ζ-potential of the micelle changed from negative to positive to improve cellular entry in acidic TME[14]. Although promising, these negative to positive charge-reversal nanoparticles are not suitable for effective and stable loading of negatively charged nucleic acid drugs. Nucleic acid drugs show great potential to improve tumor immunogenicity in cancer immunotherapy[16], including polyinosinic-polycytidylic acid [Poly(I:C)][17], CpG oligodeoxynucleotides[18], 2′,3′-cGAMP[19], messenger RNA vaccines[20] and

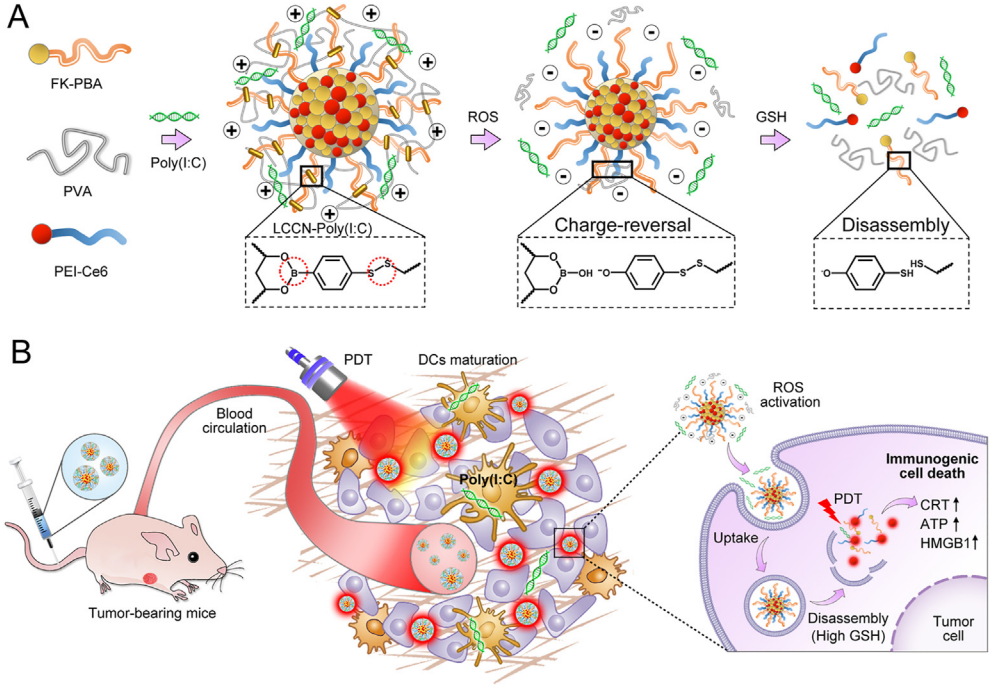

Scheme 1 Schematic illustration of the LCCN and its mechanisms for enhanced photodynamic immunotherapy against TNBC. (A) Design of LCCN-Poly(I:C). Briefly, FK-PBA, PVA and PEI-Ce6 are self-assembled into nanoparticles and then load Poly(I:C) *via* electrostatic interactions. The release of Poly(I:C) is actively controlled by NIR light *via* a charge-reversal process. LCCN-triggered ROS promote the cleavage of phenylboronic ester between PBA and PVA, and then lead to the variation of surface charge. The nanoparticles are totally disassembled in reduction microenvironment owing to the break of disulfide bond in FK-PBA. (B) The nanoparticles distribute into tumors after intravenous injection. Poly(I:C) is released from the nanoparticles once irradiated by 655 nm NIR light. When combined with PDT-induced ICD, the nanoparticles efficiently prime antitumor immune responses and inhibit the growth of 4T1 tumors in mice.

small interfering RNA (siRNA) that targeting immune pathways[21,22]. Generally, cationic polymers are used to condense the nucleic acid drugs into nanoparticles *via* electrostatic interactions. Cationic polymer/nucleic acid complexes enable stable loading and efficient internalization into tumor cells, while prevent dissociation in cytoplasm[23−25]. The complexes hamper the release of nucleic acid drugs, resulting in deactivation, degradation and decreased efficacy[26]. It remains a challenge to develop new cationic nanocarriers for delivering nucleic acid-based immune modulators with efficient drug release property.

Herein, we designed a near-infrared (NIR) light-controllable charge-reversal nanoparticle (LCCN) to co-deliver toll-like receptor 3 (TLR3) agonist Poly(I:C) and photosensitizer chlorin e6 (Ce6) for enhancing photodynamic immunotherapy of TNBC. The nanoparticles are self-assembled by using 9-fluorenyl methoxycarbonyl (Fmoc)-KCRGDK-phenylboronic acid (FK-PBA), polyvinyl alcohol (PVA) and cationic polyethylenimine-derived Ce6 (PEI-Ce6), which enable effective loading of anionic Poly(I:C) (Scheme 1A). LCCN trigger reactive oxygen species (ROS) generation with NIR light irradiation and sequentially induce the cleavage of phenylboronic ester groups between FK-PBA and PVA[27]. The presence of anionic boron and oxygen anion post NIR light will lead to a positive to negative charge-reversal of LCCN and release Poly(I:C). Moreover, disassembly of LCCN can be further promoted in reduction microenvironment due to breakage of disulfide linkage in FK-PBA. LCCN will distribute into tumors, activate dendritic cells (DCs), induce immunogenic cell death (ICD) of tumor cells, boost antitumor immunity and inhibit the growth of TNBC tumors (Scheme 1B). The charge-reversal nanoparticles provide a promising controlled-release strategy to deliver nucleic acid-based immune modulators, which may enhance photodynamic cancer immunotherapy of TNBC.

2. Materials and methods

2.1. Materials

Fmoc-KCRGDK peptide (FK) was purchased from Bankpeptide Biological Technology Co., Ltd. (Hefei, China). Ce6, mercaptophenylboronic acid, 2,2′-dipyridyl disulfide, 1-ethyl-3-(3-dimethylaminopropyl)carbodiimide hydrochloride (EDCI), hydroxybenzotriazole (HOBT) and lipopolysaccharide were obtained from J&K Chemicals (Beijing, China). Annexin V-FITC/propidium iodide (PI) apoptosis detection kit was obtained from Meilunbio. Co., Ltd. (Dalian, China). Polyethyleneimine (MW = 800 Da) and 2′,7′-dichlorfluorescein-diacetate (DCFH-DA) were gained from Sigma−Aldrich (Shanghai, China). PVA polymer (MW = 47/67/125 kDa) was purchased from Aladdin Co., Ltd. (Shanghai, China). Mice peripheral lymphocyte separation buffer and red blood cell lysis buffer were obtained from Dakewe Biotech Co., Ltd. (Shenzhen, China). Poly(I:C) was purchased from InvivoGen Co., Ltd. (Hong Kong, China). CD3e-PerCP-Cy5.5 (clone 145-2C11), CD8a-FITC (clone 53−6.7), CD8a-PE (clone 53−6.7) and CD86-PE (clone GL1) antibodies were purchased from Thermo Fisher scientific Co., Ltd. (Shanghai, China). CD4-FITC (clone H129.19), CD11c-FITC (clone N418), CD80-PE (clone 16-10A1), CD86-PE-Cy7 (clone GL1), FoxP3-PE (clone MF23) and IFN-γ-FITC (clone XMG1.2) were obtained from BD Pharmingen Co., Ltd. (San Jose, USA). Other chemicals and reagents with analytical grade were purchased from Sinopharm Group Chemical Reagent Co., Ltd. (Beijing, China).

2.2. Cell lines and animals

4T1 murine breast tumor cell was obtained from the cell bank of the Chinese Academy of Sciences (Shanghai, China). The cells were cultured in complete RPMI 1640 cell culture medium containing 10% fetal bovine serum (FBS), 2.5 g/L of glucose, 0.11 g/L of sodium pyruvate, 100 U/mL of penicillin G sodium and 100 μg/mL of streptomycin sulfate. The cells were incubated at 37 °C with 5.0% CO_2 atmosphere. Four-week-old BALB/c mice (18−20 g, female) were obtained from the Shanghai Experimental Animal Center (Shanghai, China). Animal procedures were carried out under the guidelines approved by the Institutional Animal Care and Use Committee (IACUC) of the Shanghai Institute of Material Medica, Chinese Academy of Sciences.

2.3. Synthesis of FK-PBA and PEI-Ce6

To synthesize FK-PBA, 200 mg of mercaptophenylboronic acid and 342 mg of 2,2′-dipyridyl disulfide were reacted in methanol for 2 h, and then precipitated in *n*-hexane to obtain 4-(dipyridyl disulfide)-PBA. Then, 50 mg of the product was reacted with 200 mg of FK in methanol at 50 °C for 12 h. The FK-PBA was purified in diethyl ether and vacuum-dried for use. For PEI-Ce6 synthesis, 1.6 g of PEI, 200 mg of Ce6, 287 mg of EDCI and 203 mg of HOBT were dissolved in 20 mL of anhydrous dimethyl sulfoxide (DMSO) and reacted for 24 h in dark. Then, the product was dialyzed against DMSO and water sequentially, and lyophilized for further use.

2.4. Preparation and characterization of LCCN

To optimize the formulation of LCCN, FK-PBA was firstly incubated with PVA (MW = 47 kDa) at weight ratio of 3:1, 5:1 and 15:1. Then the product was co-precipitated with PEI-Ce6 under vortex and examined by DLS. Besides, FK-PBA was incubated with PVA of various molecular weight (47/67/125 kDa) at weight ratio of 15:1, and the diameter of LCCN was examined by DLS. In detail, FK-PBA was dissolved in DMF at a concentration of 10 mg/mL. PVA (MW = 67 kDa) was then added at a final concentration of 0.67 mg/mL. The mixture was stirred at room temperature for 1 h and then co-precipitated with 1.5 mg/mL of PEI-Ce6 at a FK-PBA to PEI-Ce6 weight ratio of 1:1 under vortex. Excess PEI-Ce6 and DMF was removed by using centrifugal filtration (molecular weight cut-off, 100 kDa, Millipore). The diameter and PDI of LCCN was characterized by DLS. The morphology of these formulations was obtained by TEM. To evaluate ROS/reduction-responsive property of LCCN, the nanoparticles were treated by 655 nm NIR light at power density of 300 mW/cm^2 for 5 min, and sequentially treated with 1 mmol/L of GSH for 10 min. The suspensions with NIR light or GSH treatments were investigated by DLS and TEM examination.

2.5. Light-controllable charge-reversal property of LCCN-Poly(I:C)

Poly(I:C) was loaded into LCCN *via* electrostatic interactions between the cationic PEI-Ce6 and anionic Poly(I:C). Briefly, Poly(I:C) solution was added into the LCCN suspensions at various weight ratio and gently shaken at 37 °C for 20 min. The diameter and ζ-

potential of LCCN-Poly(I:C) were characterized by DLS. In the meanwhile, the LCCN-Poly(I:C) nanoparticles prepared at various weight ratio was irradiated by 655 nm NIR light at a power density of 300 mW/cm^2 for 5 min. The diameter and ζ-potential of NIR light-treated suspensions were also evaluated. In order to verify whether the charge-reversal of LCCN controlled by NIR light would facilitate the release of Poly(I:C), agarose gel electrophoresis was constructed. LCCN-Poly(I:C) nanoparticles with or without NIR light treated were loaded in sample hole. The agarose gel electrophoresis was performed at a voltage of 80 V for 30 min and examined by a Bio-Rad MP Imaging System.

2.6. Intracellular uptake and phototoxicity of LCCN in vitro

To determine cellular uptake of LCCN, 4T1 tumor cells were seeded at 5×10^4 cells per well in 24-well cell culture plate for 24 h. The cells were incubated with LCCN for 0.5, 1, 2, 4 and 6 h at an identical Ce6 concentration of 2.0 μg/mL. After that, the cells were washed twice and treated by 0.4% *w/w* of trypan blue to quench extracellular fluorescence and examined by using flow cytometry. To evaluate the phototoxicity of LCCN in tumor cells, the 4T1 cells were seeded at 5×10^3 cells per well in 96-well cell culture plates for 24 h. Then, the cells were incubated with increased concentration of LCCN for 6 h and irradiated by 655 nm NIR light for 1 min at various power densities. After continuous incubation for 24 h, the viability of 4T1 cells was detected by using a CCK-8 assay kit. The cytotoxicity of FK-PBA, PEI-Ce6 and LCCN without NIR light was evaluated by using the same method. To determine the apoptosis/necrosis induced by LCCN-mediated PDT *in vitro*, 4T1 cells were seeded and co-incubated with LCCN at a final Ce6 concentration of 0.5 μg/mL. The cells were irradiated by NIR light for 1 min at a series of power densities at 6 h. The apoptosis/necrosis of 4T1 cells was detected by using a Annexin V-FITC/PI apoptosis detection kit at 24 h.

2.7. Immunogenic cell death of tumor cells

To evaluate ROS generation *in vitro*, 4T1 cells were seeded on glass dishes at 3×10^4 cells per well for 24 h. The cells were treated by LCCN at an identical 2.0 μg/mL of Ce6. Six hours later, the cells were treated with 10 μmol/L of DCFH-DA for 10 min and irradiated by NIR light at a power density of 300 mW/cm^2 for 5 min. After that, the cells were fixed in 4.0% *w/w* paraformaldehyde, stained by DAPI and examined by CLSM.

The surface exposure of CRT and cytosol release of HMGB1 was detected by immunofluorescence staining. 4T1 cells were treated with LCCN at an identical Ce6 concentration of 2.0 μg/mL for 6 h and irradiated by NIR light at various power densities. Six hours later, the cells were washed twice by cold PBS, pre-blocked by 5.0% FBS and stained with anti-CRT antibody. For HMGB1 staining, the cells and nucleus were permeabilized with 0.3% Triton X-100 for 2 h and then incubated with anti-HMGB1 antibody. The samples were stained with a FITC-conjugated secondary antibody and DAPI for 30 min, and imaged by CLSM examination. Commercially available ATP assay kit was used to determine extracellular secretion of ATP. 4T1 cells were seeded in the 24-well plate at 3×10^4 cells per well for 24 h. The cells were treated with LCCN at Ce6 concentration of 0.25 or 2 μg/mL for 6 h and irradiated by 655 nm laser for 1 min. After incubating for another 12 h, the supernatant of cell culture medium was collected and ATP assay kit was used to determine extracellular secretion of ATP according to manufacturer's instructions.

2.8. Biodistribution of the LCCN-Poly(I:C)

4T1 tumor-bearing BALB/c mice were used to investigate the biodistribution of the formulation *in vivo*. 4T1 cells were injected at the right mammary of mice to estabilish the tumor models. Briefly, the mice were treated with 100 μL of LCCN or LCCN-Poly(I:C) at equal Ce6 concentration of 1.0 mg/kg by intravenous injection. The LCCN-Poly(I:C) were prepared at Poly(I:C) to LCCN weight ratio of 1:6. At predetermined time points, the mice were examined by IVIS (Ex/Em: 640 nm/680 nm). Meanwhile, the mice were sacrificed at 12 and 24 h, respectively. The distribution of nanoparticles in all major organs (heart, lung, liver, spleen, and kidney) and tumors was also examined. In order to evaluate the capacity of LCCN to deliver Poly(I:C) to tumor, 5-FAM labelled negative control nucleotides (NC) was used to prepare LCCN-NC. 4T1 tumor-bearing mice were treated with free NC or LCCN-NC at an equal NC dose of 2.0 mg/kg by intravenous injection. The mice were sacrificed at 4 h and the tumors were harvested, followed by frozen section and CLSM imaging.

2.9. Immunoassay

4T1 tumor-bearing mice at the right mammary were used to examine the immune responses induced by LCCN-Poly(I:C). Firstly, mice were intravenously injected with the desired formulations at an equal Ce6 of 2.5 mg/kg or Poly(I:C) dose of 2.4 mg/kg respectively, and treated with NIR light at 300 mW/cm^2 for 5 min in desired groups 4 h after injection. On Day 7, the tumors were harvested. Tumors were incised into small pieces and immersed in solution containing 30 U/mL DNase, 100 U/mL hyaluronidase and 175 U/mL collagenase IV. The mixture was incubated at 37 °C for 30 min, filtered through a 75 μm filter and enriched by using lymphocyte separation medium. Finally, lymphocytes separated from tumors were stained with antibodies according to the manufacturer's protocols and analyzed by flow cytometry.

2.10. Tumor models and antitumor treatments

4T1 murine breast cancer models were used to investigate the antitumor effect of LCCN-Poly(I:C). Briefly, 1×10^6 4T1 tumor cells were subcutaneously injected in the right mammary gland of 4-week-old female BALB/c mice. When tumor volume reached 100 mm^3, the mice were randomly divided into five groups: PBS, Poly(I:C), LCCN, LCCN + Laser and LCCN-Poly(I:C) + Laser group. The mice were intravenously injected with desired formulations at equal Ce6 dose of 2.5 mg/kg or Poly(I:C) dose of 2.4 mg/kg, respectively. Four hours later, the tumors were treated with NIR light at a power density of 300 mW/cm^2 for 5 min in desired groups. The treatments were repeated on Day 7. On Day 10, 5×10^5 4T1 tumor cells were injected into the left flank of each mouse to establish the abscopal tumor model. The growth of primary and abscopal tumors and body weight of mice were recorded every 2 days. The tumor volume was calculated according to the following Eq. (1):

$$\text{Volume} = \text{Longest dimension} \times \text{Shortest dimension} \times \text{Shortest dimension}/2 \quad (1)$$

The death point was set as the primary tumor volume reached 2000 mm^3 or pathological behaviors appeared in mice. At the end of antitumor study, all major organs (*i.e.*, heart, liver, spleen, lung and kidney) and tumors were harvested and fixed in 4.0% formalin solution. The organs were then dehydrated and examined by H&E

staining, while tumors were sliced for H&E, TUNEL, immunofluorescence and immunohistochemistry staining assay.

2.11. *Statistical analysis*

Data are given as the mean ± standard deviation (SD). The statistical significance was displayed by one-way ANOVA with Tukey's post hoc test and two-sided unpaired Student's *t*-test. Comparisons of survival rates were calculated by the log-rank (Mantel−Cox) test. Statistical significance was set as follows: $^{*}P < 0.05$, $^{**}P < 0.01$, $^{***}P < 0.001$.

3. Results and discussion

3.1. *Preparation and characterization of LCCN*

The FK-PBA and PEI-Ce6 was synthesized according to our previous work[28]. Briefly, 4-mercaptophenylboronic acid was conjugated to the cysteine residue of Fmoc-KCRGDK peptides *via* a disulfide linkage to get FK-PBA (Supporting Information Fig. S1). PEI-Ce6 was obtained *via* an amide condensation reaction between the amino groups of PEI and carboxyl groups of Ce6 (Supporting Information Fig. S2). To prepare the LCCN, FK-PBA was first react with PVA polymers (MW = 47 kDa) at various mole ratios, and then precipitated with PEI-Ce6 under vortex. Covalent bonds formed between PBA and diols of PVA facilitated the formation and the stability of LCCN[27]. It was found that the mole ratio between FK-PBA and diols of PVA molecules significantly affected the formation of LCCN. Both the size and polydispersity index (PDI) of the LCCN was high at mole ratios of 1:5 and 1:3, while the size and PDI of LCCN were sharply decreased to 198.7 ± 2.6 nm and 0.177 at a mole ratio of 1:1 (Fig. 1A). Next, we tested the impacts of PVA molecular weight on particle size. The diameter of LCCN could be further compressed by using PVA with higher molecular weight, approximately 113.4 ± 2.7 nm with 67 kDa and 103.7 ± 1.8 nm with 125 kDa (Fig. 1B). The loading ratio of Ce6 in these nanoparticles was 17.6 ± 0.3% and 14.4 ± 0.2%, respectively (Supporting Information Fig. S3). All formulations were examined by transmission electron microscopy (TEM) (Fig. 1C). FK-PBA alone could not form uniform nanoparticles as abundant nanofibers were observed in view, which was consistent with our previous work[28]. All groups integrated with PVA formed spherical nanoparticles and superior uniformity was achieved by using PVA at 67 or 125 kDa. Thus, we used PVA polymers at 67 kDa to prepare the LCCN in following studies.

Next, we investigated the light-controllable disassemble capacity of LCCN by dynamic light scattering (DLS) and TEM examination. Nanoparticles could be observed in TEM images of LCCN post NIR light treatment, while polymeric aggregates appeared in the same field of view. The polymeric aggregates around the nanoparticles could be the stripped PVA polymers due to ROS-induced cleavage of phenylboronic ester bonds between FK-PBA and PVA. The nanoparticles were disappeared after sequential addition of 1 mM glutathione (GSH), which could due to the breakage of disulfide linkage in FK-PBA (Fig. 1D). Consistently, a decrease of ~20 nm in LCCN diameter was detected after irradiated by

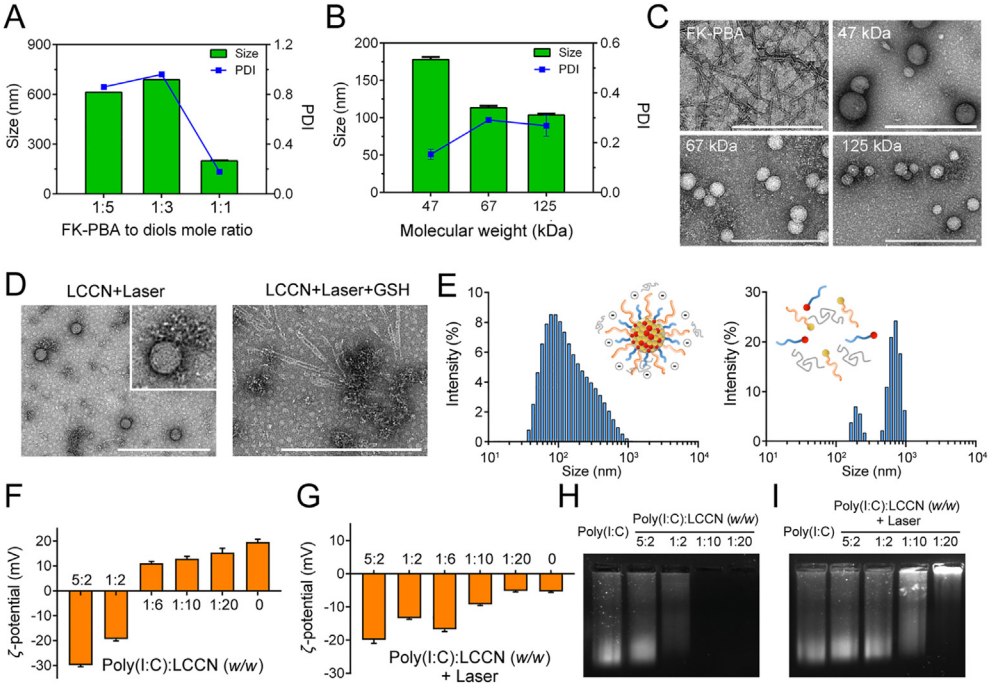

Figure 1 Preparation and characterization of LCCN and LCCN-Poly(I:C). (A) Diameter and PDI of LCCN as a fucntion of FK-PBA to diols in PVA mole ratio. (B) Diameter and PDI of LCCN when fabricated by using 47, 67 and 125 kDa of PVA. (C) TEM images of LCCN fabricated by using 47, 67 and 125 kDa of PVA. Scale bar = 500 nm. (D) TEM images of LCCN with NIR light irradiation (left) and GSH (right) treated. Scale bar = 500 nm. (E) DLS examination of LCCN with NIR light irradiation (left) and GSH (right) treated. (F) ζ-potential variation of LCCN-Poly(I:C) at different Poly(I:C) to LCCN weight ratios. (G) ζ-potential variation of LCCN-Poly(I:C) nanoparticles after NIR light irradiation at a power density of 300 mW/cm^2 for 5 min. (H) Agarose gel electrophoresis of LCCN-Poly(I:C) without NIR light treatment. (I) Agarose gel electrophoresis of LCCN-Poly(I:C) post NIR light treatment. Data are presented as mean ± SD (n = 3).

655 nm laser at a power density of 300 mW/cm^2 for 5 min, while the diameter was drastically enlarged after treated by GSH (Fig. 1E). In the presence of ROS and GSH, both the phenylboronic ester and disulfide linkage were cleaved, resulting in the disassembly of LCCN and release of Poly(I:C), PEI-Ce6, PVA as well as Fmoc-KCRGDK peptides. The $\pi-\pi$ stack interaction between Fmoc groups in peptides might promote the assemble of Fmoc-KCRGDK into nanofibers, which has been observed in our previous study[29]. Since the release of Fmoc-KCRGDK was triggered after laser irradiation, it would not influence the efficacy of Poly(I:C) and Ce6-based PDT effects. To investigate the light-controllable charge-reversal feature of LCCN for effectively controlled release of nucleic acid drugs, we loaded anionic TLR3 agonist Poly(I:C) onto the cationic LCCN at various weight ratios. The diameter of LCCN was not affected by the loading of Poly(I:C) (Supporting Information Fig. S4). With the increased Poly(I:C) to LCCN ratio, the ζ-potential of LCCN-Poly(I:C) showed a decrease manner due to the increased negative charge intensity of Poly(I:C) (Fig. 1F). The ζ-potential of LCCN-Poly(I:C) was 11.1 ± 0.7 mV at Poly(I:C) to LCCN ratio of 1:6. Interestingly, the ζ-potential of LCCN-Poly(I:C) was drastically reversed from positive to negative at Poly(I:C) to LCCN ratios < 1:2 after NIR light treatment (Fig. 1G), showing a light-controllable charge-reversal property. Gel shift assay of the LCCN-Poly(I:C) nanoparticles performed a consistent manner with the ζ-potential variation. The LCCN failed to load all Poly(I:C) molecules at Poly(I:C) to LCCN ratios ≥ 1:2 as shift bands of Poly(I:C) was observed. No electrostatic shift band was observed at ratios <1:2 without NIR light (Fig. 1H). Oppositely, obvious shift bands were performed at ratios <1:2 after irradiated by NIR light at 300 mW/cm^2 for 5 min (Fig. 1I), indicating the charge-reversal of LCCN promoted the release of Poly(I:C). With Poly(I:C) to LCCN ratio at 1:6, striking contrast was observed between groups with or without NIR light irradiation (Supporting Information Fig. S5A). The release of Poly(I:C) in LCCN-Poly(I:C) nanoparticles was barely influenced by incubating with 1.0% of fetal bovine serum (FBS) for 24 h (Fig. S5B). The diameter of LCCN-Poly(I:C) nanoparticles was slightly increased after incubating with 1.0% of FBS for 2 h, potentially due to the adsorption of certain proteins onto the surface of nanoparticles (Fig. S5C). To verify the universality of this light-controllable charge-reversal behavior for effective release of other kinds of nucleotides, we performed ζ-potential examination and gel shift assay on LCCN-siRNA nanoparticles as well. Similar outcomes were obtained and more obvious shift bands were displayed with NIR light irradiation due to much uniform molecular weight of the siRNA than Poly(I:C) (Supporting Information Fig. S6). Above results indicated that the LCCN were feasible to trigger effective release of nucleic acid-based immune modulators with a light-controllable charge-reversal manner.

3.2. *Phototoxicity and immunogenic cell death of 4T1 tumor cells in vitro*

Given the effective loading of Ce6 in LCCN, we evaluated the phototoxicity of the nanoparticles on 4T1 tumor cells *in vitro*. The cellular internalization of LCCN showed a time dependent manner (Fig. 2A, Supporting Information Fig. S7). LCCN induced ~10% decrease of cell viability at 11.4 μg/mL (equal to 2.0 μg/mL of Ce6) after 24 h incubation, which could attribute to the cytotoxicity of PEI-Ce6 in LCCN (Supporting Information Fig. S8). The phototoxicity of LCCN relied on the concentration of Ce6 and power density of NIR light, as significant cytotoxicity was found even with 0.5 μg/mL of Ce6 and 200 mW/cm^2 of NIR light (Fig. 2B). After NIR light treated, bright fluorescent ROS signals was detected by using ROS probe 2,7-dichlorofluorescein diacetate (DCFH-DA), but little ROS was generated in cells without NIR light irradiation (Fig. 2C). The LCCN-based photodynamic effects induced tremendous necrosis of 4T1 tumor cells at power density over 200 mW/cm^2 as examined by Annexin V/PI staining (Fig. 2D). Accordingly, ~90% of tumor cells were necrotic after treated by 300 and 400 mW/cm^2 of laser. PDT was considered as a feasible strategy to generate immunogenic cell death (ICD). PDT-triggered immunotherapy with immune checkpoint blockade has offered a potential appealing paradigm to eradicate tumors[30]. ICD was featured by surface exposure of calreticulin (CRT), cytosol release of high mobility group box 1 (HMGB1) and extracellular release of adenosine triphosphate (ATP)[31]. We investigated LCCN-based photodynamic effect for inducing ICD in 4T1 tumor cells. Increasing exposure of CRT (Fig. 2E) and cytosol release of HMGB1 (Fig. 2F) were generated at 6 h following elevated power density of NIR light (Supporting Information Fig. S9). Obvious fluorescent signals from HMGB1 were detected in nucleus of tumor cells without laser irradiation. However, it was found that HMGB1 leaked from nucleus into cytoplasm with 200 mW/cm^2 laser, indicating LCCN-based PDT induced efficient ICD in 4T1 tumor cells with laser power density ≥200 mW/cm^2. The level of extracellular ATP was also significantly elevated by NIR light treatment at 12 h with 200 mW/cm^2 and 2.0 μg/mL of Ce6 (Fig. 2G). Since ATP was produced in living cells, 400 mW/cm^2 of laser induced more rapid and drastic necrosis of tumor cells, potentially reducing the production of ATP as well as the extracellular leakage *in vitro*. These results suggested that LCCN induced effective ICD in tumor cells, which might potentiate antitumor immune responses *in vivo*. Next, we tested the effects of LCCN-induced ICD on the maturation of DCs. 4T1 tumor cells were first treated by LCCN and NIR light for 6 h, and then co-incubated with bone marrow DCs (BMDCs). Obviously, LCCN-induced ICD promoted the maturation of BMDCs as higher expression of CD80 (Fig. 2H) and CD86 (Fig. 2I) was detected in contrast to untreated groups. These results suggested that LCCN could not only induce phototoxicity but also effectively trigger ICD *in vitro*.

3.3. *Delivery of Poly(I:C) into tumors and elicitation of antitumor immunity*

For biodistribution assay, 4T1 tumor-bearing BALB/c mice were treated with LCCN or LCCN-Poly(I:C) suspensions and examined by *in vivo* imaging system (IVIS). Provably, both the nanoparticles showed effective accumulation in tumors 2 h post the injection. The fluorescent signals retained for 48 h in tumor site and no significant difference in tumors was found between the two groups (Fig. 3A). Similar results were detected *ex vivo* after the injection as comparable intensity was found in tumors of both groups at desired time points (Fig. 3B and C). To investigate whether LCCN enabled efficient delivery of nucleic acid drugs into tumors, we performed confocal laser scanning microscopy (CLSM) examination on tumor sections. Extremely weak fluorescent signals of FAM-labelled negative control (NC) nucleotides was found in free NC treated group, while obvious

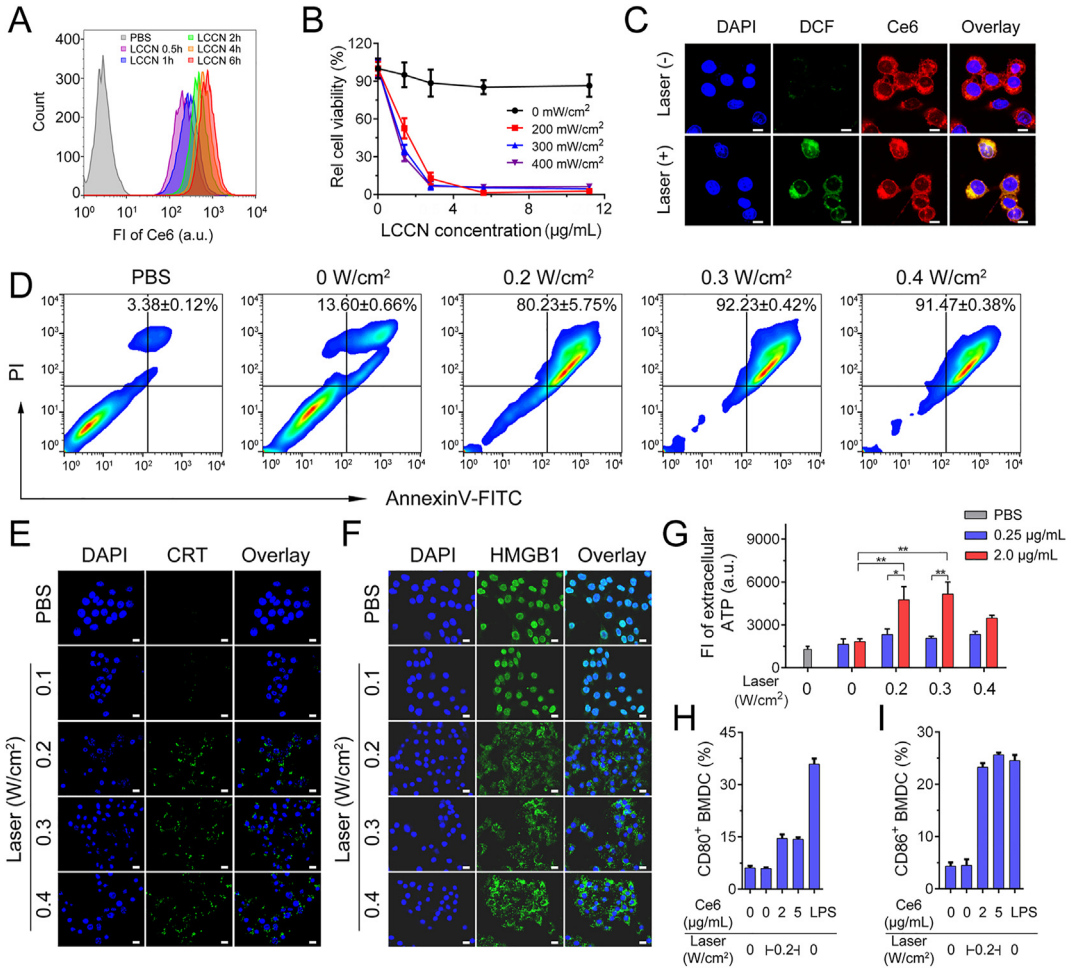

Figure 2 LCCN-induced PDT and ICD *in vitro*. (A) Intracellular uptake of LCCN after incubated with 4T1 tumor cells for 0.5, 1, 2, 4 and 6 h, respectively. (B) NIR light (655 nm) power density-dependent phototoxicity of LCCN on 4T1 tumor cells. (C) LCCN-triggered ROS prodution in 4T1 cells by using ROS probe DCFH-DA. Scale bar = 20 μm. (D) Analysis of PDT-induced apoptosis/necrosis in 4T1 tumor cells by Annexin V-FITC/PI apoptosis detection kit. (E) CRT exposure induced by LCCN-based PDT. Scale bar = 20 μm. (F) Leakage of HMGB1 from cell nucleus induced by LCCN-based PDT. Scale bar = 20 μm. (G) Extracellular secretion of ATP induced by LCCN-induced PDT at 0.25 or 2.0 μg/mL of Ce6. (H) 4T1 cells were treated with LCCN and NIR light to induce ICD. Percentage of $CD11c^+CD80^+$ BMDCs and (I) $CD11c^+CD86^+$ BMDCs was examined by flow cytometry. Data are presented as mean ± SD ($n = 3$). *$P < 0.05$, **$P < 0.01$.

green fluorescence was co-localized with Ce6 in LCCN-NC treated group (Fig. 3D). When LCCN-Poly(I:C) accumulated in tumors, the nanoparticles would be uptake by tumor cells, generate ROS, induce ICD and trigger release of Poly(I:C) as well as tumor antigens. Generally, the photodynamic effects would lead to indiscriminate killing of cells in TME, and anti-tumor immune responses were elicited following the recruitment of DCs and T cells[32]. Recruited DCs processed released tumor antigens and Poly(I:C) through endocytosis and bystander effects to improve antitumor immunity[33,34]. Besides, it was well known that protein corona was formed on the surface of nanoparticles when circulating in bloodstream[35]. The composition and content of protein varied with the surface charge, and cationic PEGylated nanoparticles could improve transvascular transport, tumor penetration and cellular internalization in contrast to anionic or neutral counterparts[36]. Optimal surface charge could be a key factor for good pharmacokinetics of nanoparticles. According to distribution results, the surface charge of LCCN-Poly(I:C) was well optimized to enable superior tumor-specific distribution while reduce the clearance of reticuloendothelial system.

As effective light-controllable charge-reversal and tumor-specific distribution could be achieved by LCCN-Poly(I:C), we tested its impacts on antitumor immune responses *in vivo*. It was well confirmed that Poly(I:C) enabled effective maturation of DCs[37]. Compared to other groups, the frequency of matured DCs in tumors was significantly elevated in mice treated by LCCN-Poly(I:C) plus laser (Fig. 3E). Moreover, the population of tumor infiltrated $CD8^+$ T cells, was ~2.9-fold higher in LCCN-Poly(I:C) plus laser group than that of PBS-treated mice. As exact ICD effects were observed *in vitro* (Fig. 2E–H), LCCN-based photodynamic effects could also improve the frequency of $CD8^+$ T cells in LCCN plus laser treated tumors (Fig. 3F). It was found that the $CD8^+$ to $CD4^+$ T cell ratios in LCCN + Laser and LCCN-poly(I:C) + Laser groups were 2.8- and 4.1-fold higher than that in PBS group, indicating that LCCN-poly(I:C)-based combination therapy efficiently activated immune responses in tumors (Supporting Information Fig. S10). The immune priming effects of PDT have been confirmed in our previous works[21,38,39]. Furthermore, the frequency of regulatory T cells (Tregs) was also

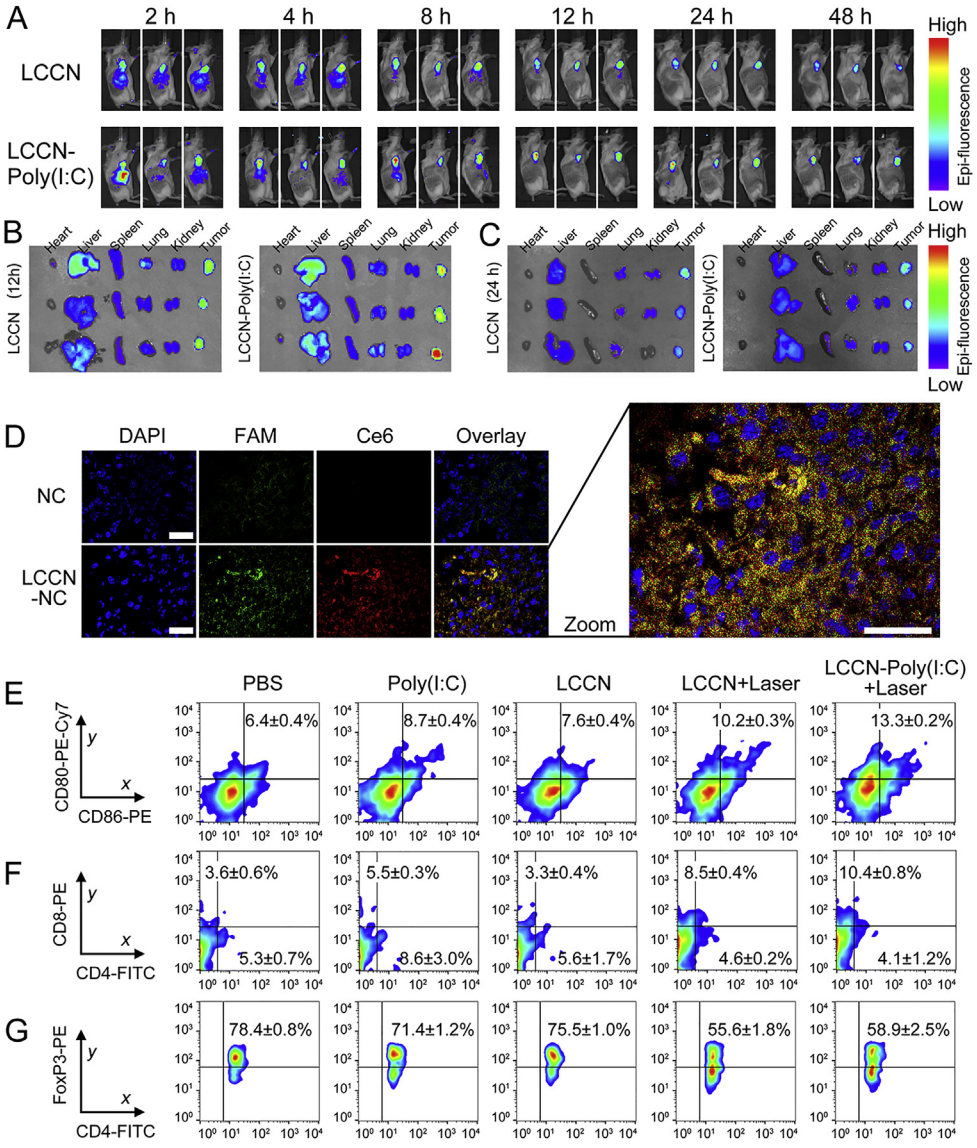

Figure 3 LCCN-Poly(I:C) effectively distributed into tumors and induced antitumor immunity in 4T1 tumor model. (A) Fluorescent imaging of LCCN and LCCN-Poly(I:C) intravenously treated mice at equal 1.0 mg/kg of Ce6. (B) Biodistribution of LCCN and LCCN-Poly(I:C) *ex vivo* at 12 h and (C) 24 h. (D) CLSM images of FAM-NC distribution in tumor sections 4 h post-injection. Scale bar = 50 μm. (E) Frequency of $CD11c^+CD80^+CD86^+$ DCs in tumors. (F) Frequency of $CD3^+CD4^+$, $CD3^+CD8^+$ T cells in lymphocytes harvested from tumors in control and treated groups. (G) Frequency of Tregs in tumors with different treatments. Data are presented as mean ± SD (n = 3).

decreased after LCCN-Poly(I:C) plus laser treated in contrast to PBS group (Fig. 3G), potentially lifting the suppressive burden of Tregs on $CD8^+$ T cells.

3.4. Photodynamic cancer immunotherapy based on LCCN-Poly(I:C) in vivo

Inspired by the high efficacy of LCCN-Poly(I:C) to prime antitumor immunity, we further evaluated the potential of this charge-reversal nanoparticles for inhibiting the growth of TNBC. 4T1 tumor-bearing mouse model is a typical type of TNBC model with aggressive metastasis feature. Plenary targeting delivery strategies have been overviewed to provide insightful thoughts on promising treatments[40]. Once the tumor volume reached 100 mm^3, 4T1 tumor-bearing mice were treated twice with different suspensions and NIR light in desired groups (Fig. 4A). Although LCCN-based PDT (LCCN + Laser group) almost totally disrupted the established 4T1 tumors during initial period, the tumors rapidly relapsed from Day 11 as raised tumor growth kinetic was observed in mice. Remarkably, enhanced antitumor effect was achieved in mice treated by LCCN-Poly(I:C) plus NIR light. The treatment delayed 96.7% of the tumor growth in contrast to PBS group, showing a significantly enhanced antitumor efficacy against 4T1 tumors (Fig. 4B). The body weight of mice was also monitored during the antitumor study. No significant difference was found between LCCN and PBS groups. Accordingly, the body weight of mice was mildly decreased after LCCN plus laser or LCCN-Poly(I:C) plus laser treated during initial period (Fig. 4C), potentially due to PDT-induced adverse effects. Fortunately, the body weight of mice in these groups was recovered over time. Moreover, the survival duration of mice was significantly prolonged with LCCN-Poly(I:C) plus laser treated

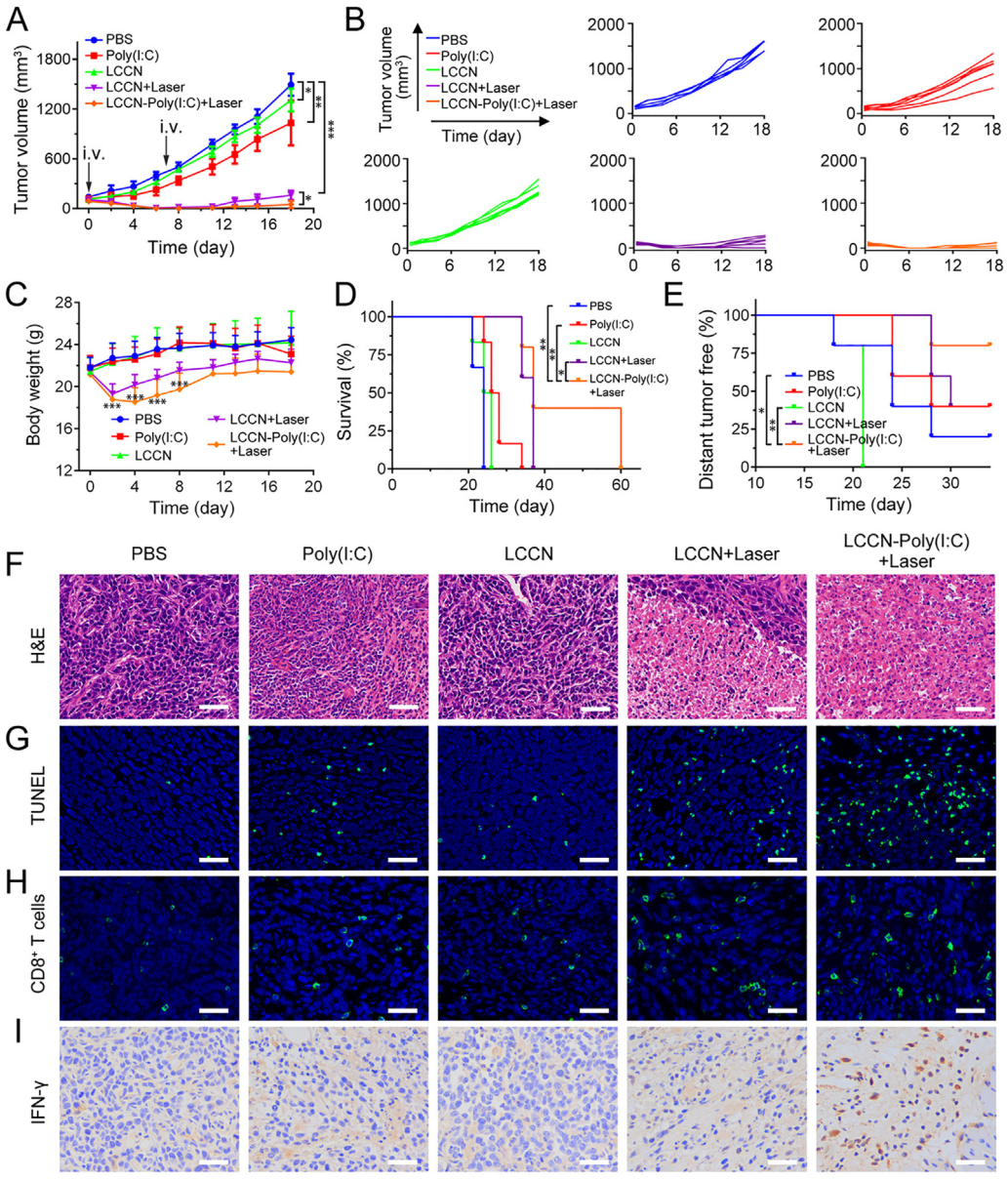

Figure 4 Growth inhibition of primary and abscopal 4T1 tumors by LCCN-Poly(I:C). (A) Average growth kinetics of primary tumors after treatments ($n = 6$). (B) Individual growth kinetics of tumors in mice. (C) Body weight ($n = 6$). (D) Survival percentage in control and treated groups ($n = 6$). (E) Abscopal tumor free percentage of mice with various treatments ($n = 5$). (F) H&E assessment of primary tumors. Scale bar = 200 μm. (G) TUNEL staining of primary tumor sections. Scale bar = 100 μm. (H) Fluorescent staining of $CD8^+$ T cells in tumor slice. Scale bar = 100 μm. (I) Histochemistry staining of IFN-γ^+ cells in tumor slice. Scale bar = 100 μm. Data are presented as mean ± SD. $^*P < 0.05$, $^{**}P < 0.01$, $^{***}P < 0.001$.

when compared with other four groups (Fig. 4D). Given that the activation of antitumor immunity in tumor site may prime systemic effect[41,42], we examined the antitumor efficacy of LCCN-Poly(I:C) on abscopal tumor model. The primary tumors were treated twice and then distant tumors were inoculated. It was found that abscopal tumors were established much earlier in mice treated with PBS or LCCN than that of LCCN-Poly(I:C) plus laser group. Eighty percent of mice were free of abscopal tumor establishment after LCCN-Poly(I:C) plus laser treated (Fig. 4E), which was obviously delayed than that with PBS or LCCN treatments.

Hematoxylin-eosin (H&E) staining of the primary tumor sections showed that both LCCN + Laser and LCCN-Poly(I:C) + Laser induced obvious cell apoptosis and necrosis, as broken nucleus and diffused cytoplasm was found in these groups (Fig. 4F). Terminal deoxynucleotidyl transferase dUTP nick-end labeling (TUNEL) examination also confirmed that more apoptotic tumor cells appeared after LCCN-Poly(I:C) plus laser treated (Fig. 4G). Besides, both $CD8^+$ T cells (Fig. 4H) and secreted IFN-γ (Fig. 4I) in tumors was elevated after the treatment, which might attribute to TLR3 activation and PDT-based ICD. Above results provided partial mechanisms that might explain the enhanced antitumor efficacy of LCCN. Besides, barely appreciable injury or inflammation was detected in the major organs (heart, liver, spleen, lung and kidney) of mice in control and treated groups (Supporting Information Fig. S11).

4. Conclusions

In this study, we have developed a charge-reversal nanoparticle which is positively charged for loading nucleotides-based immune modulators while rapidly reversed to negative charge for effective drug release under active NIR light control. With NIR light irradiation, the LCCN trigger abundant ROS and sequentially lead to the cleavage of phenylboronic ester between PBA and PVA, and then totally disassembled in reduction microenvironment. This light-controllable charge-reversal property enables active-control over the release of nucleic acid-based immune modulators loaded by LCCN. LCCN induce effective phototoxicity and ICD in 4T1 tumor cells, and highly prime the antitumor immune responses when combining TLR3 agonist Poly(I:C) *in vivo*. The nanoparticles enable efficient tumor-targeting distribution of payloads and significantly inhibit the growth of primary and abscopal 4T1 tumors. The novel approach is applicable to deliver broad types of nucleic acid-based immune modulators with effective release property, which provides a promising strategy to treat TNBC with enhanced photodynamic cancer immunotherapy.

Acknowledgments

Financial supports from the National Natural Science Foundation of China (81903548, 81690265, 81803444, 81521005 and 32070927), the Youth Innovation Promotion Association of CAS (2019283), the Strategic Priority Research Program of CAS (XDA12050307), Shandong Provincial Natural Science Foundation (ZR2019ZD25), the International Partnership Program of CAS (153631KYSB20190013) and the Shanghai Sailing Program (19YF1457300) are gratefully acknowledged.

Author contributions

Dangge Wang and Lei Fang designed the project. Lei Fang did the experiment and data analysis. Zitong Zhao, Jue Wang, Ping Xiao and Xiangshi Sun helped with immunoassay and antitumor studies *in vivo*. Prof. Yaping Ding and Prof. Pengcheng Zhang provided technical helps for the experiment. Dangge Wang and Prof. Yaping Li supervised, wrote and reviewed the final manuscript. All of the authors have read and approved the final manuscript.

Conflicts of interest

The authors have no conflicts of interest to declare.

Appendix A. Supporting information

Supporting data to this article can be found online at https://doi.org/10.1016/j.apsb.2021.06.006.

References

1. Bianchini G, Balko JM, Mayer IA, Sanders ME, Gianni L. Triple-negative breast cancer: challenges and opportunities of a heterogeneous disease. *Nat Rev Clin Oncol* 2016;**13**:674−90.
2. Merino D, Weber TS, Serrano A, Vaillant F, Liu K, Pal B, et al. Barcoding reveals complex clonal behavior in patient-derived xenografts of metastatic triple negative breast cancer. *Nat Commun* 2019;**10**:766.
3. Yin L, Duan JJ, Bian XW, Yu SC. Triple-negative breast cancer molecular subtyping and treatment progress. *Breast Cancer Res* 2020;**22**:61.
4. Shigematsu H, Kadoya T, Masumoto N, Sasada T, Emi A, Ohara M, et al. The efficacy and safety of preoperative chemotherapy with triweekly abraxane and cyclophosphamide followed by 5-fluorouracil, epirubicin, and cyclophosphamide therapy for resectable breast cancer: a multicenter clinical trial. *Clin Breast Cancer* 2015;**15**:110−6.
5. Schneeweiss A, Mobus V, Tesch H, Hanusch C, Denkert C, Lubbe K, et al. Intense dose-dense epirubicin, paclitaxel, cyclophosphamide *versus* weekly paclitaxel, liposomal doxorubicin (plus carboplatin in triple-negative breast cancer) for neoadjuvant treatment of high-risk early breast cancer (GeparOcto-GBG 84): a randomised phase III trial. *Eur J Cancer* 2019;**106**:181−92.
6. Barroso-Sousa R, Keenan TE, Pernas S, Exman P, Jain E, Garrido-Castro AC, et al. Tumor mutational burden and pten alterations as molecular correlates of response to PD-1/L1 blockade in metastatic triple-negative breast cancer. *Clin Cancer Res* 2020;**26**:2565−72.
7. Savas P, Loi S. Expanding the role for immunotherapy in triple-negative breast cancer. *Cancer Cell* 2020;**37**:623−4.
8. Tan T, Wang YQ, Wang J, Wang ZW, Wang H, Cao HQ, et al. Targeting peptide-decorated biomimetic lipoproteins improve deep penetration and cancer cells accessibility in solid tumor. *Acta Pharm Sin B* 2020;**10**:529−45.
9. Stirrups R. Pembrolizumab for triple-negative breast cancer. *Lancet Oncol* 2020;**21**:E183.
10. D'Abreo N, Adams S. Immune-checkpoint inhibition for metastatic triple-negative breast cancer: safety first?. *Nat Rev Clin Oncol* 2019;**16**:399−400.
11. Schmid P, Cortes J, Pusztai L, McArthur H, Kummel S, Bergh J, et al. Pembrolizumab for early triple-negative breast cancer. *New Engl J Med* 2020;**382**:810−21.
12. Jia WF, Wang YS, Liu R, Yu XR, Gao HL. Shape transformable strategies for drug delivery. *Adv Funct Mater* 2021;**31**:2009765.
13. Liu J, Iqbal S, Du XJ, Yuan YY, Yang XZ, Li HJ, et al. Ultrafast charge-conversional nanocarrier for tumor-acidity-activated targeted drug elivery. *Biomater Sci* 2018;**6**:350−5.
14. Dai LL, Li X, Duan XL, Li MH, Niu PY, Xu HY, et al. A pH/ROS cascade-responsive charge-reversal nanosystem with self-amplified drug release for synergistic oxidation-chemotherapy. *Adv Sci* 2019;**6**:1801807.
15. Li FY, Du Y, Liu JA, Sun H, Wang J, Li RQ, et al. Responsive assembly of upconversion nanoparticles for pH-activated and near-infrared-triggered photodynamic therapy of deep tumors. *Adv Mater* 2018;**30**:1802808.
16. Guo Q, Jiang C. Delivery strategies for macromolecular drugs in cancer therapy. *Acta Pharm Sin B* 2020;**10**:979−86.
17. Phuengkham H, Song C, Um SH, Lim YT. Implantable synthetic immune niche for spatiotemporal modulation of tumor-derived immunosuppression and systemic antitumor immunity: postoperative immunotherapy. *Adv Mater* 2018;**30**:1706719.
18. Wang C, Sun WJ, Wright G, Wang AZ, Gu Z. Inflammation-triggered cancer immunotherapy by programmed delivery of cpg and anti-PD1 antibody. *Adv Mater* 2016;**28**:8912−20.
19. Shae D, Becker KW, Christov P, Yun DS, Lytton-Jean AKR, Sevimli S, et al. Endosomolytic polymersomes increase the activity of cyclic dinucleotide STING agonists to enhance cancer immunotherapy. *Nat Nanotechnol* 2019;**14**:269−78.
20. Miao L, Li LX, Huang YX, Delcassian D, Chahal J, Han JS, et al. Delivery of mRNA vaccines with heterocyclic lipids increases anti-tumor efficacy by STING-mediated immune cell activation. *Nat Biotechnol* 2019;**37**:1174−85.
21. Wang DG, Wang TT, Liu JP, Yu HJ, Jiao S, Feng B, et al. Acid-activatable versatile micelleplexes for PD-L1 blockade enhanced cancer photodynamic immunotherapy. *Nano Lett* 2016;**16**:5503−13.
22. Deng H, Tan SW, Gao XQ, Zou CM, Xu CF, Tu K, et al. *Cdk5* knocking out mediated by CRISPR-Cas9 genome editing for PD-L1 attenuation and enhanced antitumor immunity. *Acta Pharm Sin B* 2020;**10**:358−73.
23. Van Bruggen C, Hexum JK, Tan Z, Dalai RJ, Reineke TM. Nonviral gene delivery with cationic glycopolymers. *Accounts Chem Res* 2019;**52**:1347−58.

24. Li ZY, Ho W, Bai X, Li FQ, Chen YJ, Zhang XQ, et al. Nanoparticle depots for controlled and sustained gene delivery. *J Control Release* 2020;**322**:622−31.
25. Xu CF, Li DD, Cao ZT, Xiong MH, Yang XZ, Wang J. Facile hydrophobization of siRNA with anticancer drug for non-cationic nanocarrier-mediated systemic delivery. *Nano Lett* 2019;**19**: 2688−93.
26. Charbe NB, Amnerkar ND, Ramesh B, Tambuwala MM, Bakshi HA, Aljabali AAA, et al. Small interfering RNA for cancer treatment: overcoming hurdles in delivery. *Acta Pharm Sin B* 2020;**10**: 2075−109.
27. Stubelius A, Lee S, Almutairi A. The chemistry of boronic acids in nanomaterials for drug delivery. *Accounts Chem Res* 2019;**52**: 3108−19.
28. Fang L, Zhao Z, Wang J, Zhang P, Ding Y, Jiang Y, et al. Engineering autologous tumor cell vaccine to locally mobilize antitumor immunity in tumor surgical bed. *Sci Adv* 2020;**6**:eaba4024.
29. Wang T, Wang D, Yu H, Feng B, Zhou F, Zhang H, et al. A cancer vaccine-mediated postoperative immunotherapy for recurrent and metastatic tumors. *Nat Commun* 2018;**9**:1532.
30. Hu C, He XQ, Chen YX, Yang XT, Qin L, Lei T, et al. Metformin mediated PD-L1 downregulation in combination with photodynamic-immunotherapy for treatment of breast cancer. *Adv Funct Mater* 2021;**31**:2007149.
31. Duan XP, Chan C, Lin WB. Nanoparticle-mediated immunogenic cell death enables and potentiates cancer immunotherapy. *Angew Chem Int Ed* 2019;**58**:670−80.
32. Yang WJ, Zhang FW, Deng HZ, Lin LS, Wang S, Kang F, et al. Smart nanovesicle-mediated immunogenic cell death through tumor microenvironment modulation for effective photodynamic immunotherapy. *ACS Nano* 2020;**14**:620−31.
33. Yuan P, Hu XG, Zhou QX. The nanomaterial-induced bystander effects reprogrammed macrophage immune function and metabolic profile. *Nanotoxicology* 2020;**14**:1137−55.
34. Zhou Q, Shao SQ, Wang JQ, Xu CH, Xiang JJ, Piao Y, et al. Enzyme-activatable polymer−drug conjugate augments tumour penetration and treatment efficacy. *Nat Nanotechnol* 2019;**14**:799−809.
35. Lee H. Effects of nanoparticle electrostatics and protein−protein interactions on corona formation: conformation and hydrodynamics. *Small* 2020;**16**:1906598.
36. Wang HX, Zuo ZQ, Du JZ, Wang YC, Sun R, Cao ZT, et al. Surface charge critically affects tumor penetration and therapeutic efficacy of cancer nanomedicines. *Nano Today* 2016;**11**:133−44.
37. Nagato T, Lee YR, Harabuchi Y, Celis E. Combinatorial immunotherapy of polyinosinic-polycytidylic acid and blockade of programmed death-ligand 1 induce effective CD8 T-cell responses against established tumors. *Clin Cancer Res* 2014;**20**:1223−34.
38. Feng B, Hou B, Xu ZA, Saeed M, Yu HJ, Li YP. Self-amplified drug delivery with light-inducible nanocargoes to enhance cancer immunotherapy. *Adv Mater* 2019;**31**:1902960.
39. Wang DG, Wang TT, Yu HJ, Feng B, Zhou L, Zhou FY, et al. Engineering nanoparticles to locally activate T cells in the tumor microenvironment. *Sci Immunol* 2019;**4**:eaau6584.
40. Zhang W, Wang F, Hu C, Zhou Y, Gao HL, Hu J. The progress and perspective of nanoparticle-enabled tumor metastasis treatment. *Acta Pharm Sin B* 2020;**10**:2037−53.
41. Meng ZQ, Zhou XF, Xu J, Han X, Dong ZL, Wang HR, et al. Light-triggered in situ gelation to enable robust photodynamic-immunotherapy by repeated stimulations. *Adv Mater* 2019;**31**:1900927.
42. Zhang PC, Zhai YH, Cai Y, Zhao YL, Li YP. Nanomedicine-based immunotherapy for the treatment of cancer metastasis. *Adv Mater* 2019;**31**:1904156.